Design of Machines and Structures, Vol. 10, No. 2 (2020), pp. 73–84.
https://doi.org/10.32972/dms.2020.017

DRAG COEFFICIENT CALCULATION OF MODIFIED MYRING-SAVONIUS WIND TURBINE WITH NUMERICAL SIMULATIONS

MAHMOUD SALEH – ENDRE KOVÁCS

University of Miskolc, Department of Physics and Electrical Engineering
3515 Miskolc-Egyetemváros
mhmodsalh84@gmail.com; kendre01@gmail.com

Abstract: Nowadays the importance of renewable energy is growing, and the utilization of the low wind energy potential is getting crucial. There are turbines with low and high tip speed ratio. Turbines with low tip speed ratio such as the Savonius wind turbine can generate adequate amount of torque at low wind velocities. These types of turbines are also called drag machines. The geometry of the blade can greatly influence the efficiency of the device. With Computational Fluid Dynamics (CFD) method, several optimizations can be done before the production. In our paper the Savonius wind turbine blade geometry was designed based on the so-called Myring equation. The primary objective of this paper was to investigate the drag coefficient of the force acting on the surface of the blade. Also, the Karman vortex was investigated and the space ratio of that vortex in our simulation was compared to a typical one. The power coefficient of a new Savonius turbine was investigated at different values of top speed ratio (TSR). For the sake of simplicity, a *2D* cross-sectional area was investigated in the simulation with ANSYS Fluent 19.2.

Keywords: *Savonius wind turbine, Myring Equation, CFX, CFD*

1. INTRODUCTION

Wind turbine is a device which converts the kinetic energy from the wind to another form of energy by a mechanical mechanism. They consist of blades which rotate around an axis due to the wind force. There are many classifications of the wind turbines. According to the nature of the force used to produce the torque, wind turbines can be classified as “lift-wind turbines” or “drag-wind turbines” [1]. The mean reason behind developing Drag-Wind Turbines is that they work regardless of wind direction. Drag-Wind Turbines do not need a yaw mechanism. This makes them ideal for small-scale usage such as remote areas with very small electric load. Their blades do not need a mechanism to change their angle when they operate with any wind direction. The small size means they can be integrated easily within an urban setting and present no danger to the wildlife in rural areas. The most commonly used Drag-Wind Turbine is the Savonius wind turbine. The Savonius wind turbine was created by Savonius in 1922. It is most basic design in an S-shape with two blades. The Savonius turbine depends on the drag force to push the blade to produce a torque which will make the rotor work. Aerodynamically it is the simplest wind turbine to

design and build which decreases its cost completely compared to other blades of the other wind turbines. Its working principle is extremely simple. The turbine revolves because of the difference in the values of the drag force acting on the concave and convex surfaces of its blades as shown in *Figure 1*.

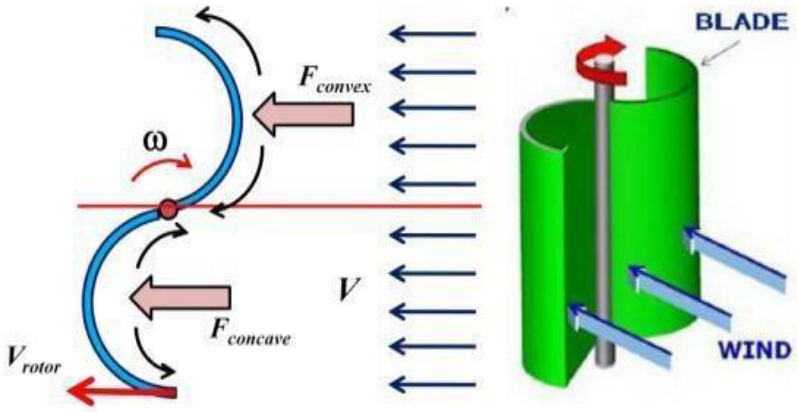

Figure 1
Working principle of a Savonius rotor

The air enters the concave surface and pushes the turbine. The flow that hits the convex surface does generate a drag which is lower than the force acting on the concave surface. It is the difference in the values of the drag forces that enables the turbine to work. The experimental study of E. Aymane [2] refers that Savonius wind turbines work well at low wind velocities (cut in speed at around 2.5 $m\ s^{-1}$). According to the same study, two blades operate better than three blades since more drag is dissipated in the three blades versions. The power coefficient of the two-blade design is higher than that of the three-blade design. The aim of this paper is to introduce a new design of the blade of the Savonius wind turbine and investigate the power and drag coefficients.

2. METHOD

Even though 2D-simulations fail to consider the 3D-simulation effects, previous studies have shown that two-dimensional simulations give acceptable results for Savonius Turbines [3]. Therefore, the three-dimensional effects are ignored, and two-dimensional transient simulations are carried out to reduce the time cost in this study. The simulations were done using Ansys Fluent 19.2.

2.1. Modified Savonius-Myring Blade

The net force which pushes the Savonius blade and produces the torque depends on two forces which are $\boldsymbol{F_{convex}}$ and $\boldsymbol{F_{concave}}$ as shown in *Figure 1*. The net torque increases when $\boldsymbol{F_{concave}}$ increases but it decreases when the $\boldsymbol{F_{convex}}$ increases. The

main goal of our study is to decrease the drag force acting on the convex surface of the Savonius blade and also increase the drag force acting on the concave surface so that we can enhance the efficiency of the turbine. Among many factors, the geometry of the blade is the critical factor in determining the value of those forces. In our study we chose to generate the surfaces based on the Myring Equation. It is widely used in the design of submarines working under the water and it is reported that it gives ideal results [4]. The formula of the Myring Equation in the Cartesian Coordinates is:

$$\boldsymbol{y = b\left[1 - \left(\frac{x}{a}\right)^2\right]^{\frac{1}{n}}}, \tag{1}$$

here a, b and n can be any positive number. That equation generates a wide range of geometries. When $n = 2$ it determines an ellipse and for special cases when $a = b$ it determines a circle. The parabola can be defined when the factor $a = 1$. In [3], the author defined $b = a = 0.25\ m$ and changed the value of the factor n in order to predict its influence on the efficiency. In our simulation, we held $n = 2$ and changed the factors *a* and *b*. This determined a half-ellipse shape. We connected two of them to generate the S-blade shape.

2.2. Fluid domain and Boundary conditions

For any blade with diameter *D*, and based on the study of W. Tian [3], the tunnel was given the dimensions $\boldsymbol{12D}$ wide and $\boldsymbol{18D}$ length. We chose these dimensions to make sure that the upstream flow is completely developed. The blade is placed at an equal distance between the top and the bottom boundaries, at distance $\boldsymbol{6D}$ from the inlet boundary *(Figure 2)*.

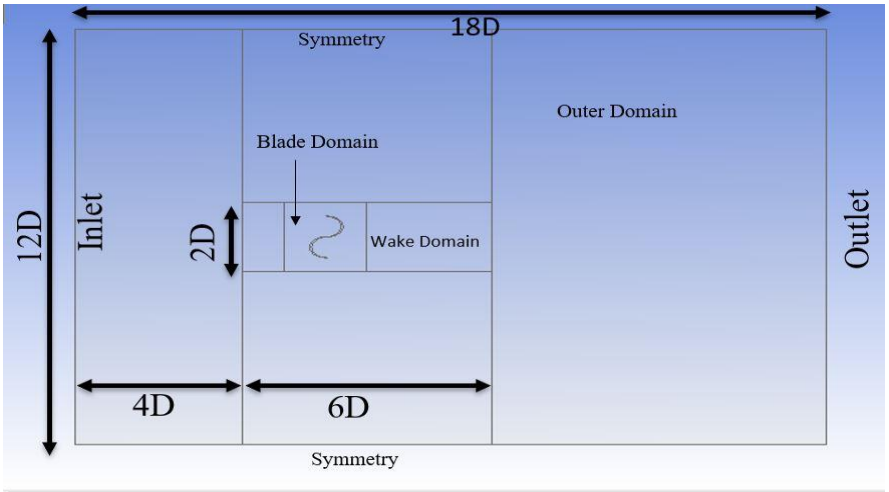

Figure 2
Fluid Domain and the boundary conditions

The whole domain was divided into three subdomains in order to control the mesh quality. The wake domain was given the dimensions $\boldsymbol{2D \times 6D}$ while the blade domain was given the dimensions $\boldsymbol{2D \times 2D}$. A uniform velocity profile was used at the inlet. The value of the inlet-velocity was set to different values for each blade, which were $\{\mathbf{3}, \mathbf{5}, \mathbf{6}, \mathbf{10}\}\ \mathbf{m\ s^{-1}}$. The pressure outlet was used at the outlet of the tunnel. No slip-wall was applied at the surface of the blade. To improve the stability of the numerical simulations, symmetry boundary conditions were applied at both the top and the bottom edges of the domain. The symmetry boundary condition is useful because it allows the solver to consider the wall as part of a larger domain.

2.3. Mesh Generation

The mesh was generated by the Mesh tool in Ansys 19.2. As mentioned before, the whole domain was divided into three subdomains in order to control the mesh quality and the aspect ratio. As we will see later, the diameters of the blades are existing in the domain $\{1, 1.2, 1.4\}m$. Taking into consideration the smallest blade diameter, the blade domain surrounding directly the blade has the finest mesh which was 10 mm, while the wake domain contains cells with 50 mm. It was generated to be able to capture the tail of the vortex in case an eddy formed. Far away from the blade in the outer domain, the resolution was the lowest. Multizone was the dominant method and the type of mesh was set as quadrilateral. *Figure 3* shows the gradient in the mesh size around the blade and outer domain. It can be seen also from *Figure 4* that the aspect ratio around the blade and in most of the domain is around 1 which is the ideal value of the aspect ratio. Even in some regions which have the highest value, the aspect ratio does not reach 6. It is known that aspect ratio with a value of 10 is still accepted. The inflation was generated around those surfaces in order to increase the accuracy of the calculations. For this purpose, the value of the $y+$ was calculated to ensure that the height of the first layer of the inflation will be less than the thickness of the boundary layer.

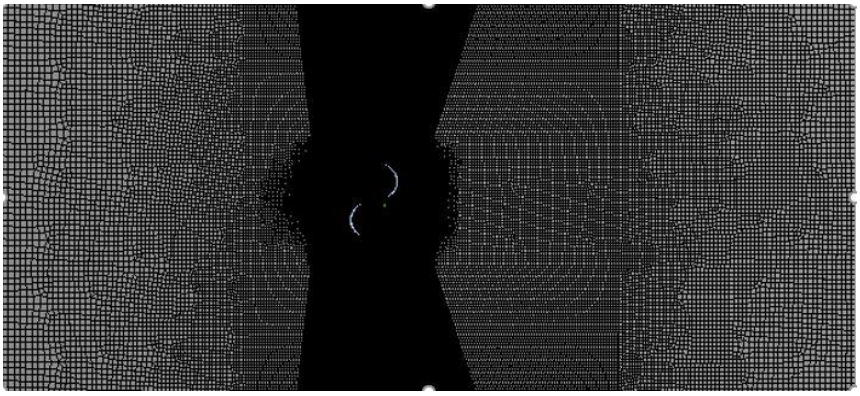

Figure 3
Generated Mesh

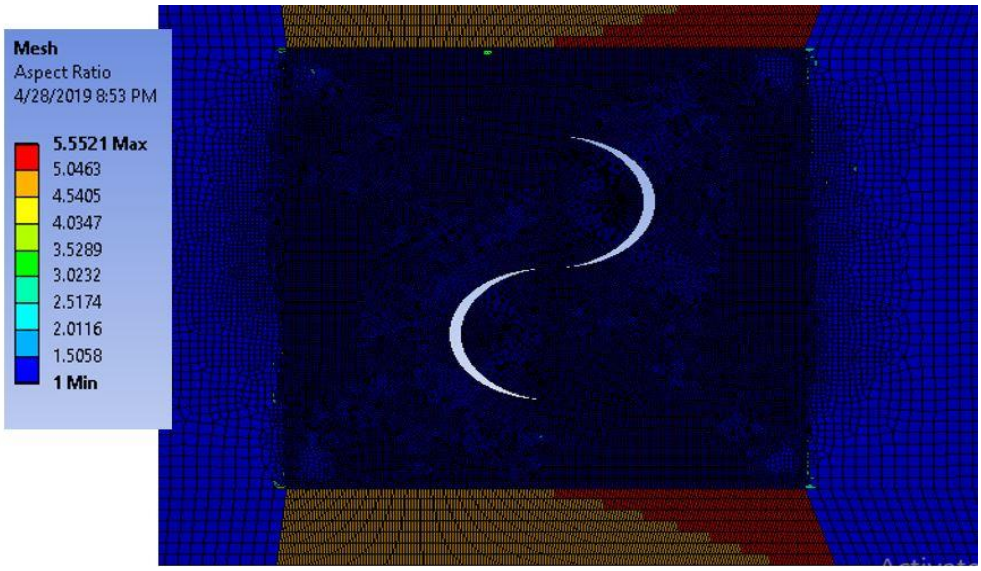

Figure 4
The aspect ratio

2.4. The Turbulence Model and Setup

Numerical (CFD) models intended to predict flow in a computational domain with the combination of Navier–Stokes equations and turbulence prediction techniques [5]. The transition SST turbulence model was applied. The transition SST model is based on the coupling of the SST $k-\omega$ transport equations with two other transport equations, one for the intermittency and one for the transition onset criteria, in terms of momentum-thickness Reynolds number. An ANSYS proprietary empirical correlation (Langtry and Menter) has been developed to cover standard bypass transition as well as flows in low free-stream turbulence environments. For transient formulation, second order implicit option was used. The value 500 was used as the number of time steps. To increase the accuracy of the calculations, the time step was set as 0.1 second. Solution was initialized with hybrid initialization. A Second Order Upwind spatial discretization algorithm was used for pressure and momentum.

2.5. Validation

To validate the method mentioned above we conducted *2D* simulations with the following values of the Myring-Equation (1): $\boldsymbol{a = b = 0.25\,m}$, $\boldsymbol{n = 2}$. This determines a half-circle with a C-shape. We connected two C-shapes to produce an S-shape with $\boldsymbol{1.2\,mm}$ thickness. These values were taken from reference [6]. We tested our model at two different velocities which were $\{\boldsymbol{7, 14}\}\ \boldsymbol{m\,s^{-1}}$. According to our simulations, the mean value of the static torque coefficient was roughly $\boldsymbol{0.25}$ in the both cases. In reference [7], the values were 0.25 and 0.22 at velocities $\boldsymbol{7\ m\,s^{-1}}$

and $\mathbf{14}\ \boldsymbol{m\ s^{-1}}$, respectively. The values in that reference can be checked in *Table 1* and *Figure 7* when $\boldsymbol{\theta = 0}$ (our turbine fixed in the tunnel in a way that made $\boldsymbol{\theta = 0}$ as shown in *Figure 2*). Taking into consideration that our simulation had been conducted on a 2D model while the experiment was conducted on a 3D-real model, the result of the simulation is a good approximation. We have to pay attention that the negative value of the static torque coefficient in our simulation does not matter since it refers only to direction of the angular velocity.

3. Results and Discussion

3.1. Drag coefficient crisis and Von Karman vortex effects

In this simulation, we studied the drag coefficient by holding $b = 0.25\ m$, $a = 0.450\ m$ and $n = 2$. It determines a half-ellipse shape, the so-called C-shape. We connected two C-shapes to produce an S-shape. The simulation was conducted on both shapes. The velocity $\mathbf{3}\ \boldsymbol{m\ s^{-1}}$ was applied at the inlet of both fluid domains. The value of the drag coefficient was defined as function of time as shown in *Figure 5*.

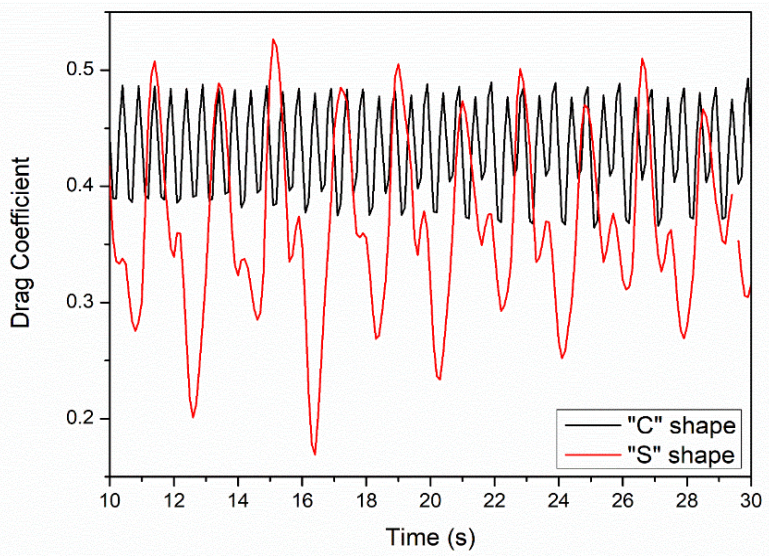

Figure 5
The drag coefficient as a function of time

In both cases, it was found that the function was changing with time. For the C-blade shape, the value of the drag coefficient changed roughly between 0.39 and 0.49 during the time interval. For the S-blade shape, the value changed in wider domain. The highest value was approximately 5.1 while the lowest value was around 0.25. For the S-blade shape, the velocity contour shows that the value of the velocity is zero along the whole surface of the blade which is called stagnation point as shown in

Figure 6. This can be explained by the fact that the kinetic energy of the fluid was converted into pressure energy. Comparing *Figure 7* with that in the study of A. Kulkarni *(Figure 1)* [8], we notice that the vortex formulated behind our blade is Karman vortex street phenomenon.

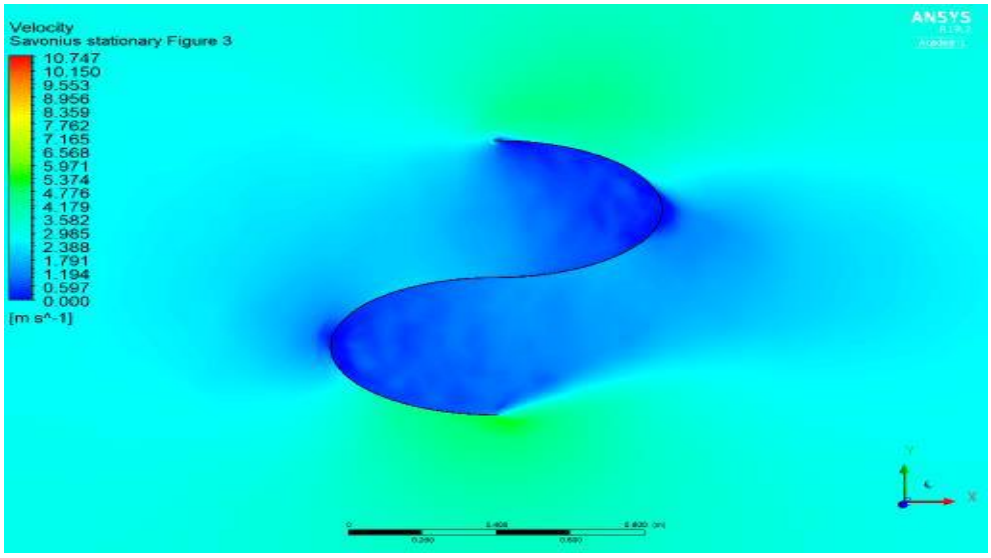

Figure 6
Velocity distribution

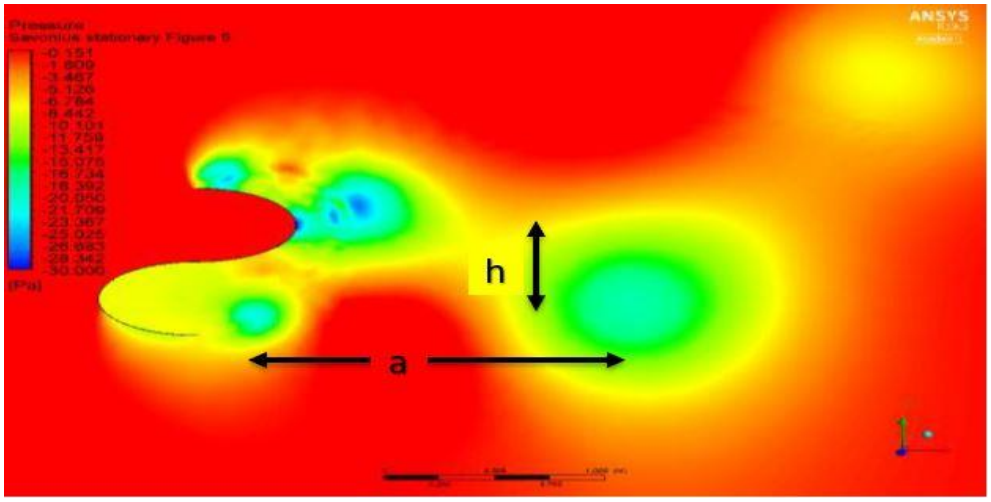

Figure 7
Karman vortex Street (Pressure Contour)

3.2. Drag Force and Drag coefficient

Holding $\boldsymbol{n = 2}$ and $\boldsymbol{a = 0.375\,m}$ while b changes in the domain $\{\boldsymbol{0.25, 0.3, 0.35}\}\boldsymbol{m}$, the Myring equation determines a half-ellipse shape the so-called C-shape. Two C-shapes were connected to produce S-blade shape with diameter $\boldsymbol{D = 4b}$. It means that $\boldsymbol{D\epsilon\{1, 1.2, 1.4\}m}$. The simulations were conducted to show the effect that the *b* factor has on both the drag coefficient and the drag force. Each an S-blade was tested at four different velocities which were {3, 5, 6, 10} $\boldsymbol{m\,s^{-1}}$. Let us denote the first blade with *b* = 0.25 m as $\boldsymbol{S_1}$, the second blade with *b* = 0.3 m as $\boldsymbol{S_2}$ and the third blade with b = 0.35 m as $\boldsymbol{S_3}$. Also, the drag force follows the renown empirical formula:

$$F = \frac{1}{2}\rho C_d V^2, \tag{2}$$

where ρ is the mass density of the fluid, C_d is the drag coefficient and V is the flow velocity relative to the object. For blade S_1, the simulations show that the drag coefficient is constant at any velocity we used. The value of the drag coefficient is $C_{d1} = 1.25$. The values of the drag force are {7, 20.1, 27, 78} N at velocities {3, 5, 6, 10}$m\ s^{-1}$ respectively. For blade S_2, the simulations show that the drag coefficient is also constant at any velocity we used. The value of the drag coefficient is $C_{d2} = 1.5$. The values of the drag force are {8.7, 25, 35, 100} N at velocities {3, 5, 6, 10} $m\ s^{-1}$ respectively. For the third blade S_3, the graph of the drag coefficient is stable at any velocity we used. The value of that drag coefficient is $C_{d3} = 2$. The drag force values are {11, 29, 40, 120}N at velocities {3, 5, 6, 10}$m\ s^{-1}$ respectively. It can be seen from *Table 1* that the drag force follows the renown empirical *Equation (2)*.

Figure 8 shows the values of the drag force at each velocity for each blade.

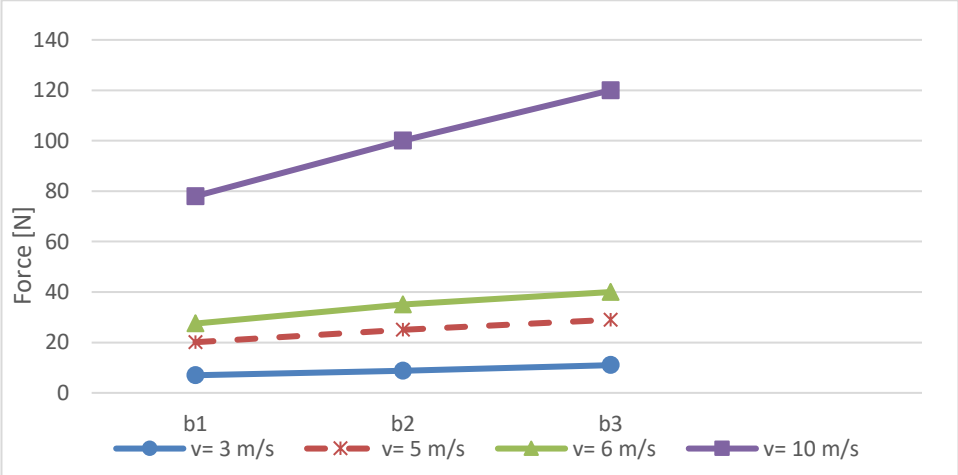

Figure 8
The drag force acting on the three blades at different velocities

In that figure, b1, b2 and b3 refer to blades S_1, S_2, S_3 respectively where the diameter of any blade is $D = 4b$. It can be clearly seen that the higher the velocity, the higher the drag force is, as it is expected. It can be also noticed that the relationship between the drag force and the diameter of the blade is linear at velocities $\{3, 5, 6, 10\}\ m\ s^{-1}$. As a result, the drag force acting on the blade with diameter between 1 m and 1.4 m and working at previous velocities can be interpolated. Also, the drag coefficient increases when the diameter of the blade increases as shown in *Figure 9*. However, the relationship is not linear in this case.

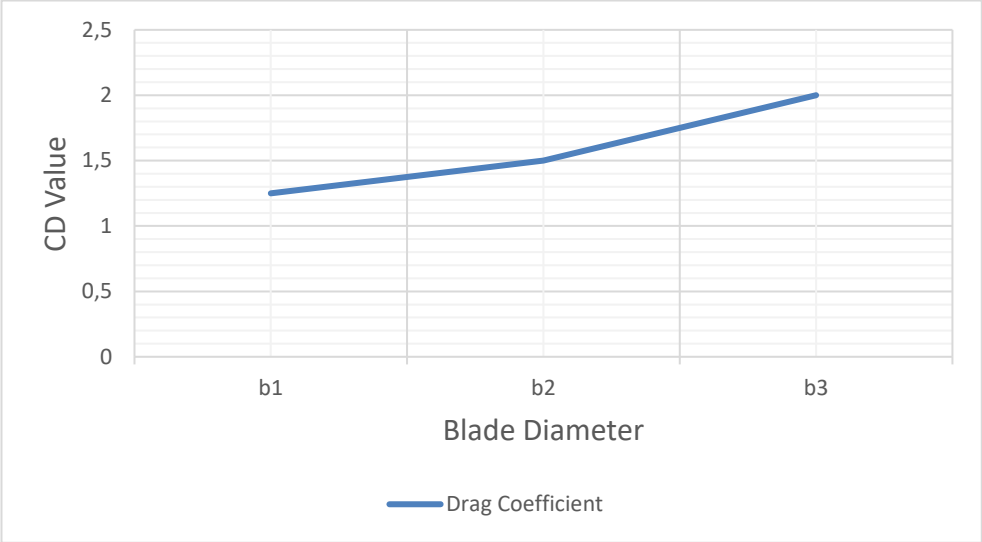

Figure 9
The drag coefficient as a function of blade diameter

Table 1
The drag force values

FORCE [N]	$V = 3\ m\ s^{-1}$	$V = 5\ m\ s^{-1}$	$V = 6\ m\ s^{-1}$	$V = 10\ m\ s^{-1}$
F_1	7	20.1	27.5	78
F_2	8.75	25	35	100
F_3	11	29	40	120

3.3. The Power Coefficient

We investigated the power coefficient of the two-blade turbine (S1 blade). A sliding mesh model was used to simulate the rotation of the rotor. The turbine was tested at different Tip Speed Ratio (TSR). Each simulation lasted for many revolutions to allow for convergence. The number of revolutions depended on the angular velocity of the turbine. Four simulations were carried out with the following values of TSR

$\{\mathbf{0.4}, \mathbf{0.6}, \mathbf{0.8}, \mathbf{1}\}$ corresponding to inlet velocities $\{\mathbf{3}, \mathbf{5}, \mathbf{6}, \mathbf{10}\}$ respectively. The Tip Speed Ratio TSR has the following formula:

$$\boldsymbol{TSR} = \frac{\boldsymbol{D\omega}}{\boldsymbol{2V}}, \tag{3}$$

where D is the diameter of the rotor ($4b$ = 1.2 m in our case), $\boldsymbol{\omega}$ is the angular velocity of the turbine and $\boldsymbol{V}$ is the inlet velocity. The power coefficient can be expressed as follows:

$$\boldsymbol{C_p = \lambda C_m}, \tag{4}$$

where C_m is the torque coefficient given by the following formula [9]:

$$C_m = \frac{4T}{\rho A_s D\, V^2}, \tag{5}$$

where T is torque, ρ is air density, A_s is the swept area, D is the turbine diameter and V is the air velocity.

Since the torque coefficient was fluctuating *(Figure 10)*, its averaged value was considered at the last revolution to allow for convergence. In Reference [3], the authors carried out simulations to investigate the power coefficient and the highest value was 0.2573 at TSR = 0.8. In our design, we can go beyond this value. At TSR = 0.8, the power coefficient was 0.28 for our turbine *Figure 11*.

Table 2

Torque coefficient with respect to TSR

λ	0.4	0.6	0.8	1
C_m C_m	0.05	0.09	0.35	0.06

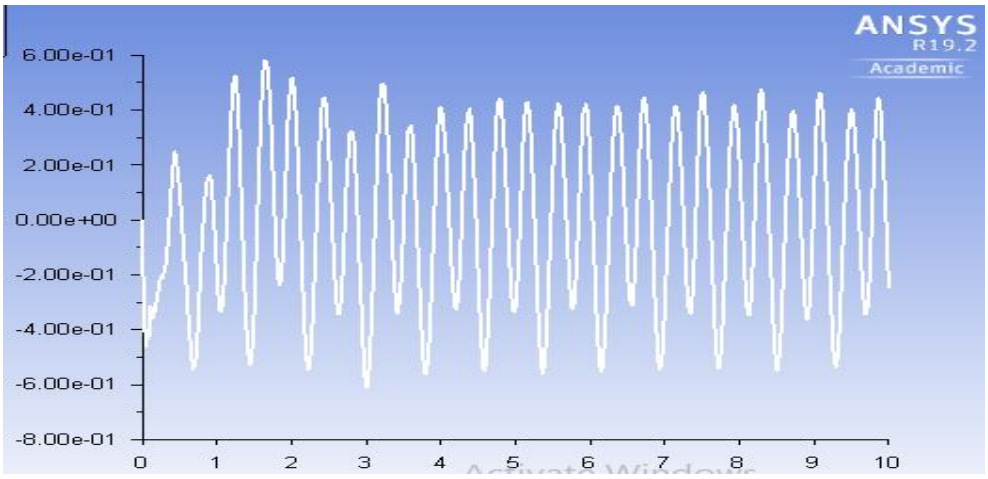

Figure 10

The torque coefficient as a function of time at TSR = 0.8

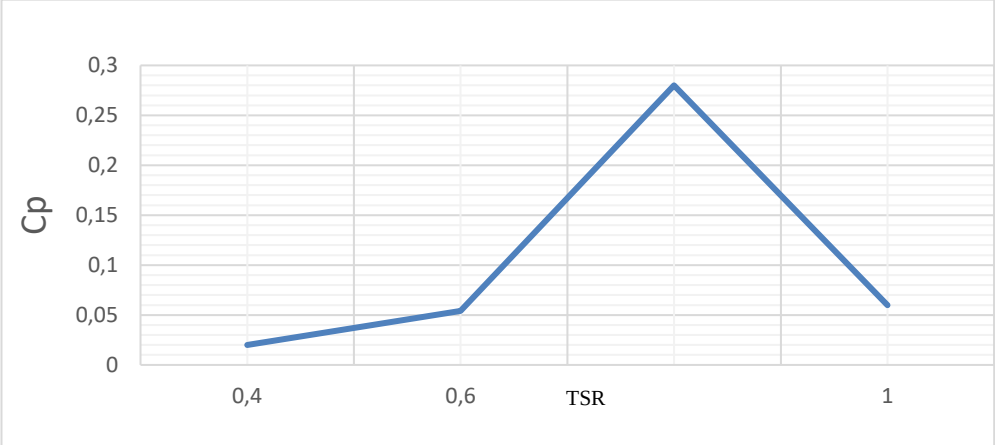

Figure 11
Power Coefficient with respect to TSR in case of the first blade S1

4. SUMMARY

The numerical simulations had been carried out to investigate Savonius wind turbine. The following results were obtained:

- The drag force and drag coefficient increase with respect to the diameter of the rotor.
- The value of the drag coefficient showed stability for the all the three cases.
- Since the relationship between the drag force and the diameter is linear, the drag force for such a design can be expected for any diameter in the domain $\{1, 1.4\}$ m.
- The simulations conducted on turbine S_1 to investigate the power coefficient showed a high value of that coefficient at TSR = 0.8. It was $C_p = 0.28$. This value is better than any value of the power coefficient that the authors obtained in reference [3].
- Although our turbine has showed a high efficiency at TSR = 0.8, it has a very low power coefficient at another TSR. So, it is suggested to be used at certain conditions to ensure that the value of TSR is close to 0.8.
- The high value of the power coefficient for the first turbine is a promising result. This encourages us to investigate this turbine more deeply. Also, the second and third turbine must be investigated.
- We have to pay attention that the values obtained from the simulations are usually higher than those obtained from laboratory. So, it is recommended to investigate our design experimentally.

REFERENCES

[1] Manwell, J. F., McGowan, J. G., Rogers, A. L. (2010). *Wind Energy Explained: Theory, Design and Application*. Vol. 2, USA, John Wiley & Sons, Ltd, 2nd edition.

[2] Aymane, E., Darhmaoui, H., Sheikh, N. (2017). *Savonius Vertical Wind Turbine: Design, Simulation and Physical Testing*. School of Science and Engineering, Alakhawany University.

[3] Tian, W., Song, B., VanZwieten, J. H., Pyakurel, P. (2015). Computational Fluid Dynamics Prediction of a Modified Savonius Wind Turbine with Novel Blade Shapes. *Energies*, Vol. 8, pp. 7915–7929.

[4] Saleh, M., Szodrai, F. (2019). Numerical Model Analysis of Myring-Savonius Wind Turbines. *International Journal of Engineering and Management Sciences*, Vol. 4, pp. 67–71.

[5] Szodrai, F. (2020). Quantitative Analysis of Drag Reduction Methods for Blunt Shaped Automobiles. *Applied Sciences*, Vol. 10, pp. 1–19.

[6] Baracu, T., Benescu, S. G. (2011). Computational Analysis of the Flow Around a Cylinder and the Drag force. In: *The 2nd Conference of the Young Researchers from TUCEB*, At Technical University of Civil Engineering of Bucharest, Bucharest, Romania, 17–18 November 2011.

[7] Blackwell, B. F., Sheldahl, R. E., Feltz, L. V. (1977). Wind Tunnel Performance Data for Two- and Three-Bucket Savonius Rotors. New Mexico, Sandia Laboratories.

[8] Kulkarni, A., Harne, M. S., Bachal, A. (2014). Study of Vortex Shedding Behind Trapezoidal Bluff Body by Flow Visualization Method. *International Journal of Engineering Research & Technology (IJERT)*, Vol. 3, No. 9, September 2014, pp. 1057–1062.

[9] Feng, F., Li, S., Li, Y., Xu, D. (2012). Torque Characteristics Simulation on Small Scale Combined Type Vertical Axis Wind Turbine. *Physics Procedia*, Vol. 24, pp. 781–786.